Marine and Petroleum Geology 151 (2023) 106089

Contents lists available at ScienceDirect

Marine and Petroleum Geology

journal homepage: www.elsevier.com/locate/marpetgeo

Review on drilling-induced fractures in drill cores

Shatavisa Chatterjee, Soumyajit Mukherjee *

Department of Earth Sciences, Indian Institute of Technology Bombay, Powai, Mumbai, 400 076, Maharashtra, India

ARTICLE INFO

Keywords:
Geomechanics
Structural geology
Deformation
Sub-surface geology
Reservoir engineering
Paleostress

ABSTRACT

Drilling-induced fractures (DIFs) develop in the drill cores as well as in the country rocks during the drilling process due to tensile failure of the rocks. A few types of DIFs can be used to decipher the far field *in-situ* stresses and to detect spatial and temporal variations in orientation of the principal stress axes. This in turn has made the study of DIFs to be crucial in the field of hydrocarbon exploration. In (sub)vertical wells, DIFs parallel the maximum horizontal stress (S_H) and are perpendicular to the breakouts. This specific geometric relation to stress field can be used to find the orientation of the S_H. Estimating principal stress directions and magnitudes are important in sand production prediction, wellbore stability, loss in fluid circulation and production-induced subsidence. Besides, DIF's orientations give a satisfactory estimate of the trend and direction of fracture propagation induced by hydraulic treatments, and the behavior of hydraulic fracturing operations during simulations. Distinguishing natural fractures from DIFs is therefore essential to identify damage zones and to model fracture network geometry of reservoirs.

1. Introduction

Drilling wells concentrate the far-field tectonic stresses around them. Drilling-induced fractures (DIFs) develop when this stress exceeds the rock strength. There are several practical reasons of studying DIFs. For example, once detected from logging and wellbore imaging, such fractures can be used to decipher the present day stress regime around them. DIFs provide a constraint on the direction of the principal stress axes and their relative magnitudes. Since DIFs are spaced usually uniformly within the core, they can also be used to extract information about the absolute magnitude of stress. The analysis of the spatial changes in widths and lengths of DIFs and the changing stress state near-the wellbore region can give clues to prevent such fractures. Additionally, accurate prediction of geometries of the early-stage fractures is important for the selection of the treatment needed to seal the DIF to prevent/minimize drilling fluid-loss and preclude additional fracturing (review in Kostov et al., 2016). Factors affecting the DIF geometry on the borehole of a well are: *(i) in-situ* stress tensor, *(ii)* relative orientations between the lines of action of stresses and the borehole, *(iii)* fluid pressures in the borehole and in the surrounding rock, *(iv)* rock's cohesive strength, and its friction angle for shear (Aadnoy and Bell, 1998).

This article reviews DIF's *(i)* morphological variations *(ii)* genesis and *(iii)* few important case studies. Examples are taken mainly from the DIFs developed in the cylindrical drill core rock samples.

2. Morphology

Various types of DIFs are of cup, disc, petal, petal centerline, saddle and scallop geometries (Fig. 1). Note that the terms *disc-shaped fractured* and the *cup-shaped fractures* have been used interchangeably in the literature. Although the morphology of the fractures may imply to a novice their genesis by tensional stress, it is quite the opposite. The stress regime required for their production is locally entirely compressive. The existing *in-situ* drilling-induced compressional stresses produce tensions that can rupture the core. DIF parallels the greatest horizontal compressive stress axis (S_H) of the local and the present-day stress regime (Zhang, 2019).

The main types of DIF morphologies are as follows (mainly as per Kulander et al., 1990).

2.1. *Disc fractures (Fig. 2)*

Disc/cup-shaped fractures mainly form in fine-grained fissile rocks due to vertical tension. These fractures are generally (sub)horizontal in a (sub)vertical core, however, their orientation can be affected by inclined beds, cross beddings and rock anisotropy. Where the rocks are foliated, disc fractures might dip toward the foliation. These fractures commonly originate between the bit and scribe knives or scribe groove. Fully

* Corresponding author.
E-mail addresses: soumyajitm@gmail.com, smukherjee@iitb.ac.in (S. Mukherjee).

https://doi.org/10.1016/j.marpetgeo.2022.106089
Received 17 September 2022; Received in revised form 22 December 2022; Accepted 23 December 2022
Available online 28 December 2022

Abbreviations

BHTV	Borehole Televiewer
DIF	Drilling-induced fracture
FMI	Formation Micro Imager
HDIL	High Definition Induction Log
KTB	German Continental Deep Drilling Project
MSCL	Multi-sensor core logger
SFIB	Stress and Failure of Inclined Boreholes
USA	The United States of America
WFSD	Wenchuan Earthquake Fault Scientific Drilling Project
3DEX	Three-dimensional expansion

Symbols

S_H	Maximum horizontal compressive stress
Φ	Angle between the cross-section and S_H
S_h	Minimum horizontal compressive stress
S_v	Overburden stress
S_b	Weight of drill bit
S_p	Fluid pressure
Pe	Photoelectric absorption factor
P_m	Downhole mud pressure
P_p	Pore pressure
T_0	Tensile strength of the rock

developed disc fractures cut across the core, whereas the incomplete ones remain hidden within the core till it is cut open.

The morphology of the disc fractures and the primary stress is influenced by the *in situ* stresses, unloading and drilling-induced torsional stresses and vibration. When unloaded, reduced overburden pressure expands the rock producing tension towards the core center. The velocity of fracture propagation increases towards the core center and decreases towards its margin. The plume axis on the disc fracture parallels S_H, thus giving an idea about the present day *in-situ* stresses (Fig. 3 and Fig. 6).

Wilson et al. (2007) documented hackle plume lines and arrest lines (Fig. 3), which show the direction of propagation of the fractures. Within the borehole, the regions with high frequency of disc fractures presumably correlate with production zones, organic content, fissility and *in-situ* stress magnitude. The disc fractures usually develop after the formation of centerline fractures (Fig. 4). Disc fractures usually break the core into short cylinders, known as *'poker chips'* or *'hockey pucks'* (Fig. 3; Lorenz and Cooper, 2017).

The stress field also affects the surface characteristic of the disc fractures. The horizontal stress anisotropy curves the disc surfaces. A more planar surface indicates that the remote stress field has a greater effect on the local stress field (Bankwitz & Bankwitz, 1997).

2.2. *Petal and petal-centerline fractures*

Petal fractures form when the magnitudes of the two horizontal principal stresses S_H and S_h ($S_H > S_h$) differ significantly. As this disparity reduces, fractures evolve from petal fractures to petal-centerline and finally reach the disc type (Li and Schmitt, 1998). A petal centerline fracture is a transverse fracture at a shallower depth, and with increasing depth it becomes centerline/longitudinal to the drill core. Also, as the vertical stress (S_V) increases during drilling, eventually petal and petal-centerline fracturing take place (Li and Schmitt, 1997a). Such fractures show two distinct morphologic sections-at one part the fracture curves down with an inclination of 30-75° at the core boundary, and superposes with the axis of the cylindrical drill core. This is followed by a centerline fracture that continues parallel to the core axis through the center of the core. The two parts of this fracture forms due to a single fracturing, and the continuous petal centerline fractures possess a common strike, which usually parallels S_H direction in case for a vertical wellbore. Kulander et al. (1990) concluded that petal fracture can occur without the centerline part, but not the vice-versa. Interestingly, Lorenz and Cooper (2017) reported a centerline fracture originating at the mid-core (Fig. 5). The centerline part of the fracture is longer than that of the petal. Neither petal nor the centerline fracture cuts across the entire core. Petal fractures initiate presumably below the cutting edge of the bit, caused by the increase in bit stress; they form before the bit during the coring process and propagate into the rock yet to be drilled (Lorenz and Finley, 1988).

The direction of propagation of DIF can be deciphered from the hackle plume features and the arrest line geometries. The propagation is usually along the arrest line that goes away from the origin and bends the least (Figs. 2 and 6a). The close-spaced arrest lines are formed due to the cyclic variation in bit pressure. This varies the tensile stresses in magnitudes and directions and propagates the fracture. In rocks with higher frequency of petal centerline fracture (e.g., Fig. 7), hydro-facturing may take place.

Although disc, petal and petal centerline fractures are more ubiquitous, other types of fractures e.g., saddle fracture (Li and Schmitt, 1998), core-edge induced fractures and sub-horizontal induced extension fractures (Wilson et al., 2007) have also been reported. A saddle-shaped disc fracture is common in a thrust fault setting where the horizontal stress magnitudes, S_H and S_h, differ considerably. The azimuth of the high points on saddle-shaped fractures lies along the direction of the least compressive stress (Fig. 1; Li and Schmitt, 1998). When the core is broken off at the completion of a run, or when the rock is relieved from load as it enters the core barrel, sub-horizontal extension fractures can develop (Wilson et al., 2007).

2.3. *Transverse DIFs*

While longitudinal DIFs (such as centerline fractures) can put a constrain on the lower bound of the S_H magnitude, transverse DIFs (e.g., cup/disc, saddle, petal) can constrain the lower bounds of both S_H and S_h. Transverse DIFs from image logs (Fig. 8) can indicate whether the stress regime is strike-slip or reverse faulting without any knowledge of S_H and S_h (Nelson et al., 2005). The factors affecting the transverse DIFs are *in situ* stress, rock strength and the weight of the drilling mud. As per the image logs, transverse DIFs are electrically conductive, non-planar and discordant to the bedding, and are confined to the tensile region of the wellbore (Nelson et al., 2005). As per Morin and Flamand (1999), disc-shaped DIFs form where drilling mud is circulated and are affected by the ephemeral thermal stresses. Nelson et al. (2005) studied the DIFs in image logs (e.g., Fig. 8) to constrain the stress regime from the West Tuna area (Australia).

3. Stress conditions for DIF formation

The morphology/type of fracture (disk, petal or petal centerline) depends on the *in-situ* stress condition of the region where the bore hole is drilled. Li and Schmitt (1998) described the different stresses acting on the borehole in different stress regimes as follows.

3.1. *Stress regimes*

3.1.1. *Normal fault regime ($S_v > S_H > S_h$)*

As per Anderson's model, $S_V > S_H$ in the normal fault regime. The high overburden stress and anisotropic horizontal stresses generate petal fractures. Petal fractures form when $S_h = 0$ and $S_H = 0.5$ (Fig. 9a) and $S_H = 0.75$ (Fig. 9b). The point of initiation of fracture is at the bottom of the drill bit since it holds the maximum tension. For $S_H \approx S_h$, petal-centerline fractures develop. These petal-centerline fractures eventually evolve into disk fractures with the increase in S_h. The strike of the petal and petal centerline fractures parallel S_H (Li and Schmitt, 1998).

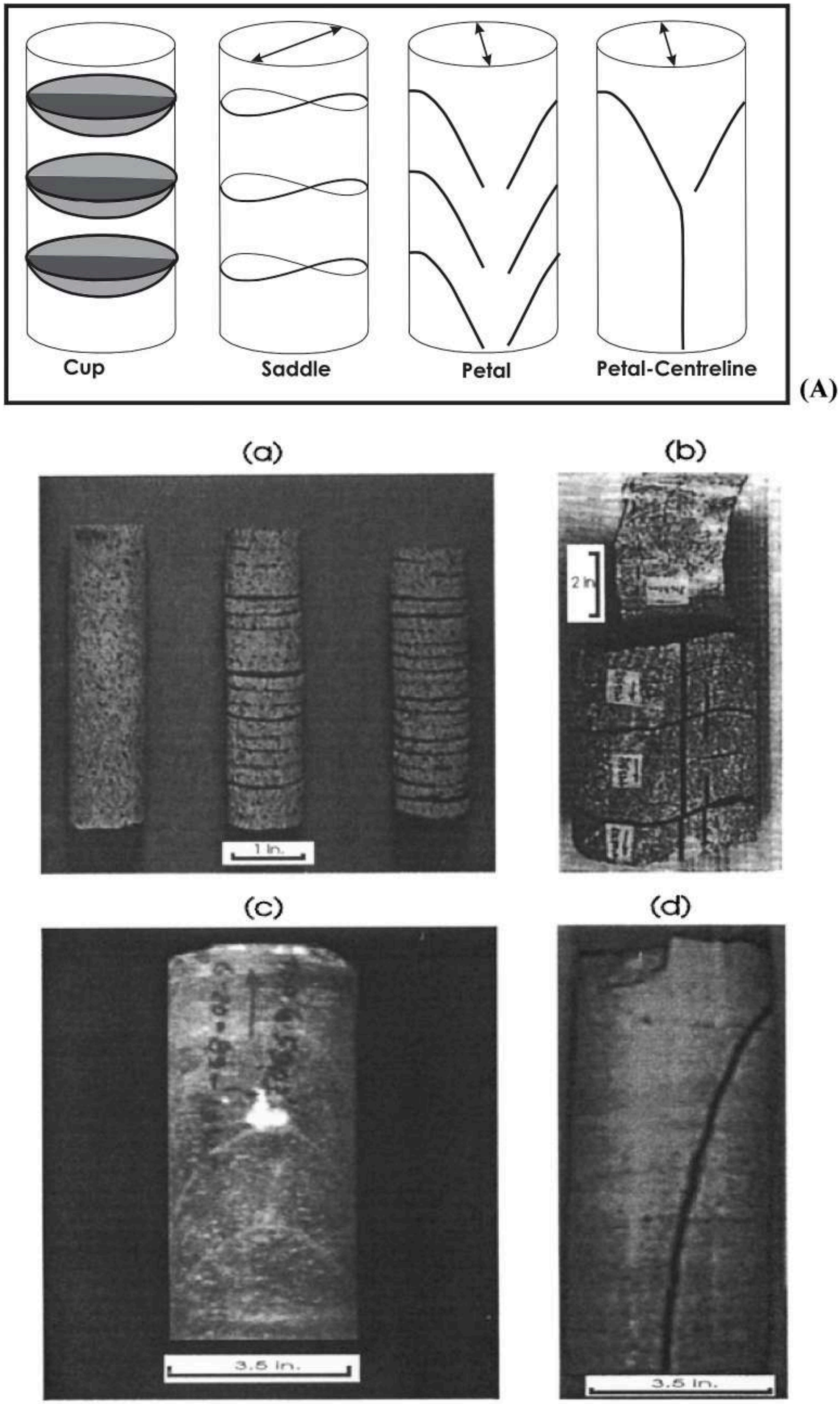

Fig. 1. A. Cartoons of common types of DIFs. Arrow: S_H direction. Reproduced from Zhang et al. (2019). Actual examples- **(a)** cup/disc fracture, **(b)** saddle fracture (e.g., Figs. 28.14 and 28.15 in Lorenz and Cooper, 2017), **(c)** petal fracture, **(d)** petal centerline fracture. Reproduced from Li and Schmitt (1998).

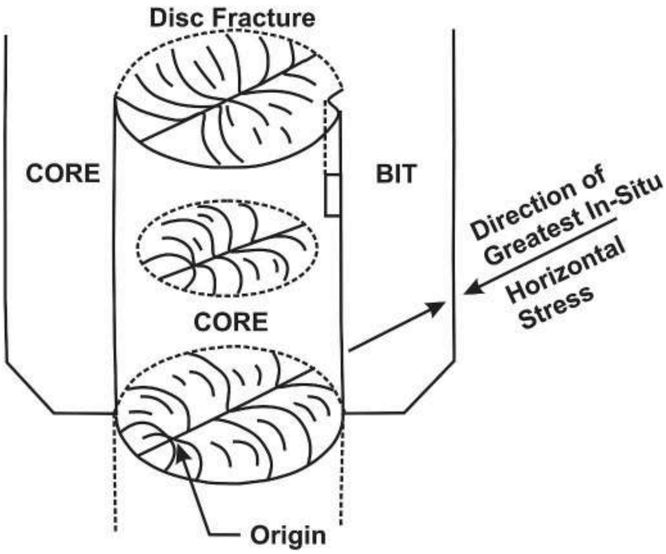

Fig. 2. Development of disc fracture. Reproduced from Kulander et al. (1990).

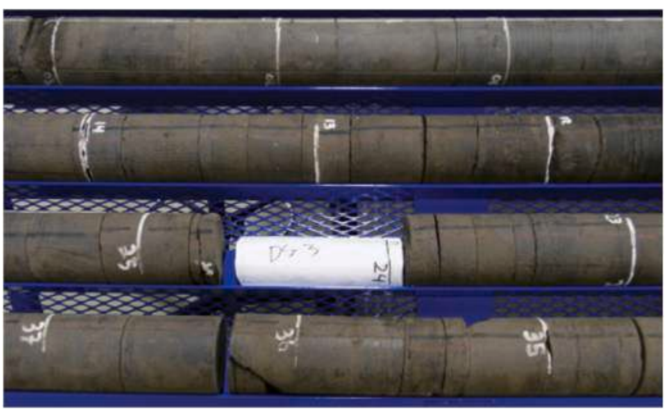

Fig. 3. Disc fractures dividing the core into poker chips' or 'hockey pucks'. Reproduced from Lorenz and Cooper (2017).

3.1.2. *Strike-slip fault regime* ($S_H > S_V > S_h$)

As per Anderson's theory, the intermediate principal stress axis is vertical (S_v) in the strike-slip regime. Fracture initiates at the bottom of the drill bit in the plane perpendicular to the maximum stress axis (S_H). As the anisotropy of the horizontal stresses, the fractures evolve from petal fractures to petal-centerline and finally become the disc type. In Fig. 10a and b, it can be seen that petal fractures form when $S_h = 0$, and $S_H = 1$ thus indicating high anisotropy between the horizontal stresses. As S_h increases to 0.17, petal center-line fractures form and at $S_h = 0.25$, disk fractures are observed. Saddle fractures are also possible along with concave (towards the sky) and nearly planar fractures *(Li and Schmitt, 1998)*.

3.1.3. *Thrust fault regime* ($S_H > S_h > S_v$)

In this type of regime (Fig. 11), $S_V < S_h$. This type of stress conditions shows a different set of fractures than the normal and the strike-slip regimes. S_H generates a large tension parallel to the inner surface of the drill bit, in the plane perpendicular to the maximum stress. Fracture initiates at the core's root. Disc-shaped fractures are the most common type under uniform horizontal stresses. In case of highly anisotropic horizontal stress, saddle-type fractures might develop, initiating at the drill bit. The fractures strike in the direction of the maximum horizontal compression and the azimuth of the high points of petal and saddle fractures lie along the S_h. This type of fracture gives an idea about the relative magnitude of the principal stresses. When S_H and S_h differ greatly, petal fractures commonly develop. As the anisotropy of the horizontal stresses decrease, fractures evolve from petal fractures to petal-centerline and finally attains a disk geometry (Li and Schmitt, 1998).

Fig. 4. Termination of discs against the centerline fractures indicate that the discs formed later. Reproduced from Lorenz and Cooper (2017).

3.2. *Components of stress inside a wellbore*

The stresses that Li and Schmitt (1997) considered in developing a finite element model for DIF formation are the horizontal stresses, overburden stress, the drill-string weight and the wellbore fluid pressure. Nonlinear phenomena, such as fluid penetration into the rock mass and fractures, torsional stress generated by drill-bit rotation and variations in rock properties e.g., Poisson's ratio were not considered.

Uniform horizontal biaxial stress causes cup-shaped disk fractures within the rock near the root of the core stub. The site of fracture

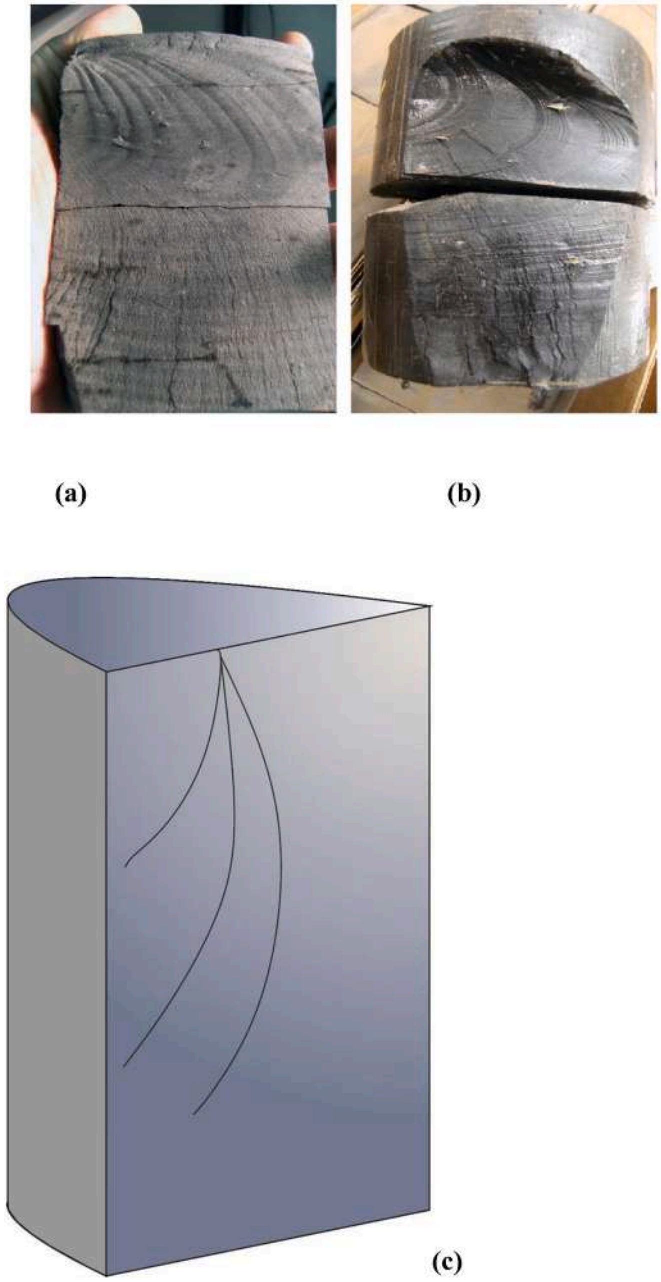

(a) (b) (c)

Fig. 5. ab. Centerline fracture originating at the mid-core. Reproduced from Lorenz and Cooper (2017). c. Sketch of Fig. 5a as seen within the drill core.

initiation changes to the surface of the core as the horizontal stresses become more anisotropic that develops saddle-shaped core discs. These fractures parallel S_H. As S_V increases during drilling, eventually petal and petal-centerline fracturing take place. According to Li and Schmitt (1997), these fractures are more close-spaced at higher stress levels. Centerline fractures produce as a combination of short core stub and high overburden stress. The maximum tensile stress increases with core stub length at first, but plateaus at ~40% of core diameter, putting maximum limits on the spacing between succeeding fractures along a core. In a biaxial stress regime, the principal stress axis is vertical along the core axis. Towards the periphery of the core, one of the principal stress axes becomes sub-vertical and develops cup-shaped core discs.

In case of hydrostatic regime, the superposition of the biaxial and overburden stresses reduces the tension inside and at the root of the core. Tensional failure occurs when the tensile strength of the rock is surpassed and the initiation of DIF occurs above the inner kerf corner.

3.3. *Effect of core length on the stress regime*

The tensile and shear stress magnitude exerted by the primary stresses (horizontal and overburden stresses, weight of drill bit and fluid pressure) increase with the length of the core stub. The stress magnitude reaches a limit when the core stub becomes 40% of the core diameter when the overburden stress (S_v) and weight of the drill bit (S_b) are considered. In case of the prevailing horizontal stresses (S_h) and fluid pressure (S_p), the limit is reached when the core stub becomes 15% of the core. The length of the core stub at which these maximum tensions occur limits the spacing of core fractures. At core stub lengths of 25% of

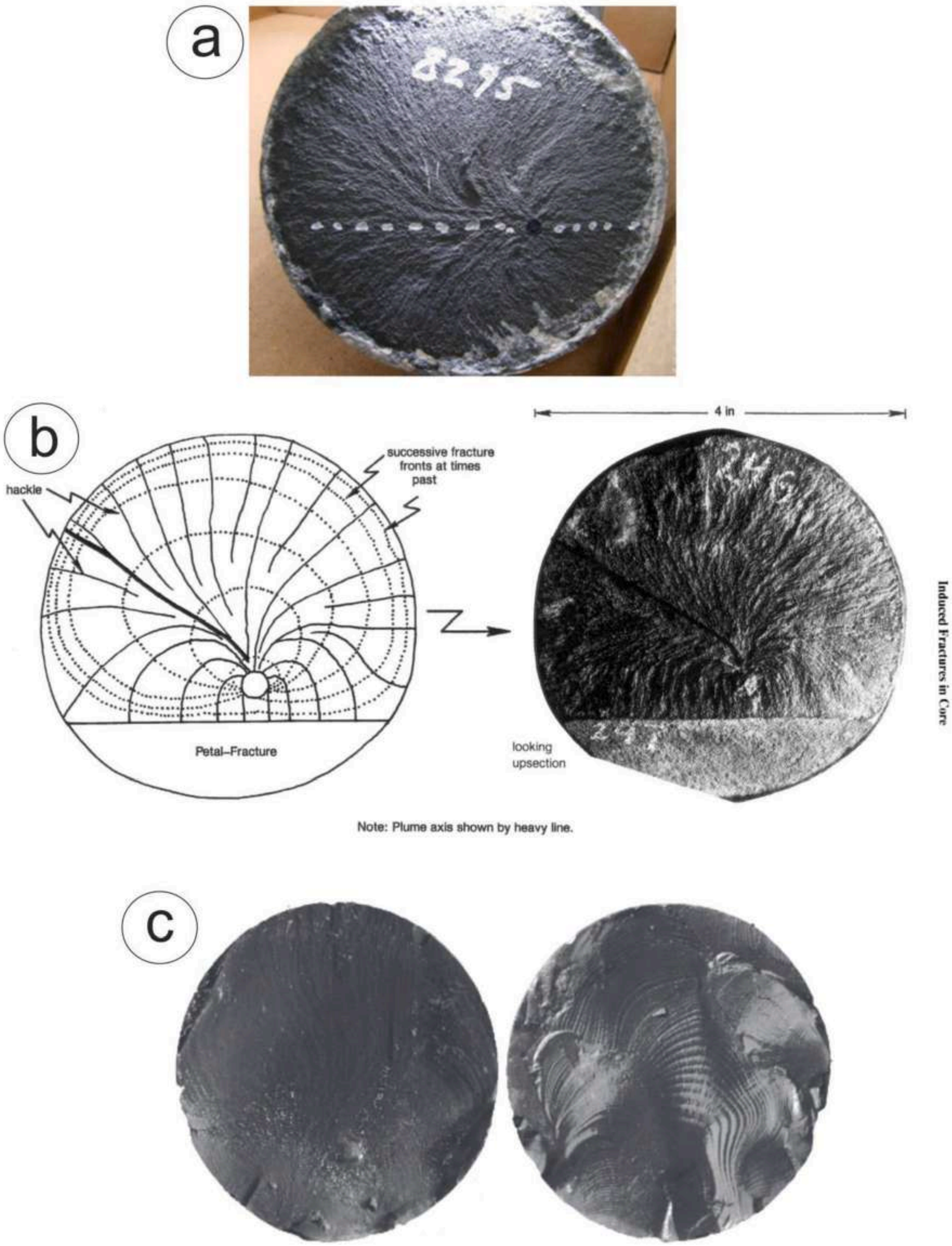

Fig. 6. Plume axis giving the direction of in-situ stress. Reproduced from (a) Lorenz and Cooper (2017), (b) Kulander et al. (1990), (c) Wilson et al. (2007).

the core diameter, most severe tensile damage may occur. If the core disking is caused by tensional damage, the discs are spaced no more than one-quarter the core diameter. This is supported by field observations and lab experiments (Li and Schmitt, 1998). Fig. 12 presents the relation between the greatest tensile stress and the normalized core-stub length.

4. DIFs in inclined and horizontal core

The classic disc and petal centerline fractures are rare in drill cores related to highly deviated or horizontal borehole due to the reorientation of the stress fields with reference to the core axis (Kulander et al., 1990). Unlike vertical wells, the principal stress axes in deviated

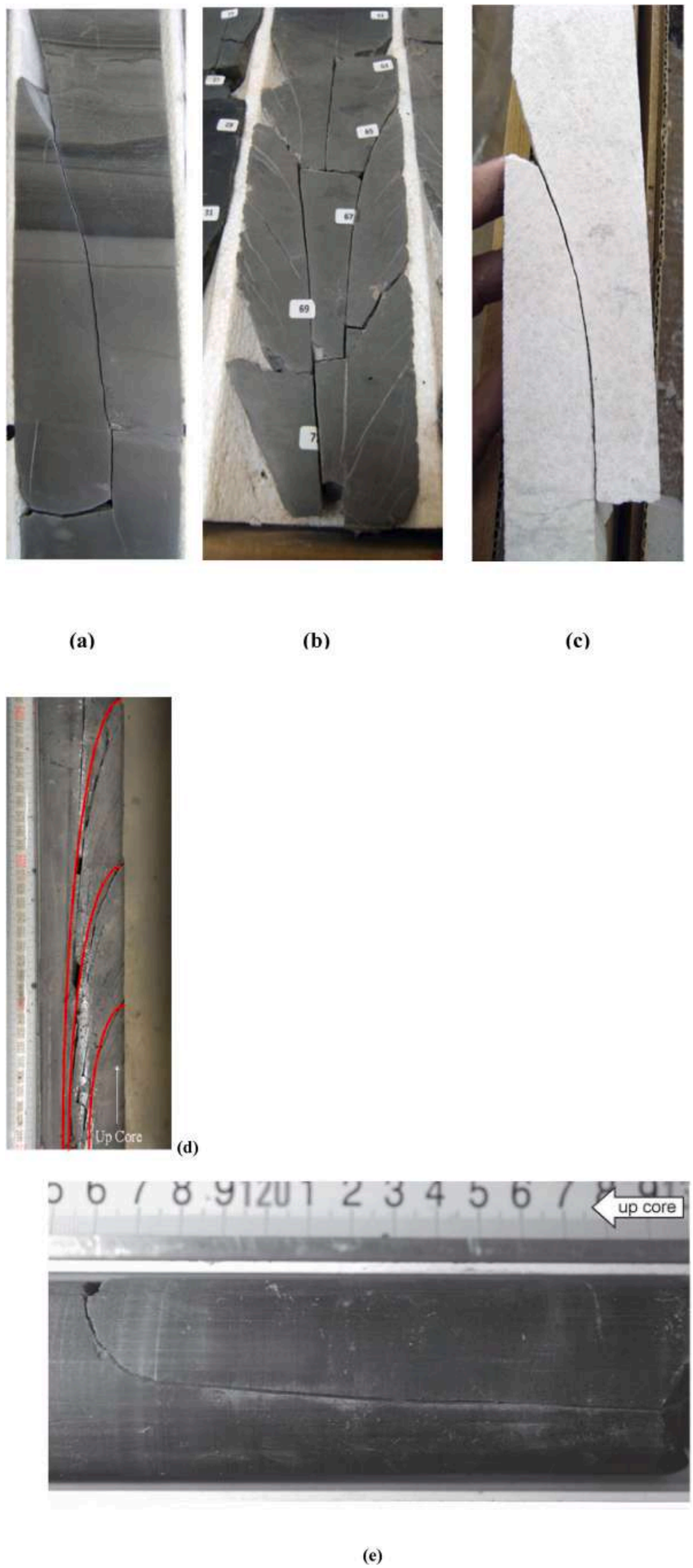

Fig. 7. Petal centerline fractures in cores. a-c. Reproduced from Lorenz and Cooper (2017). Actual petal centerline fractures in cores: d. Reproduced from Patlan et al. (2008). e. Reproduced from Wilson et al. (2007).

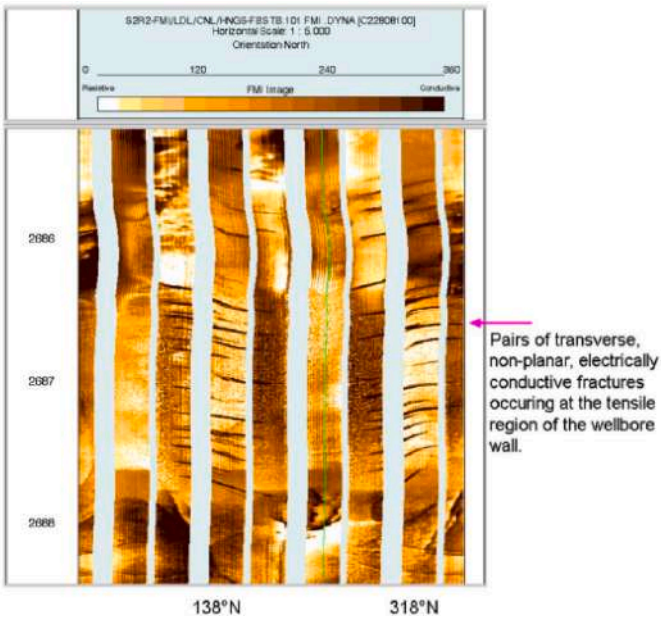

Fig. 8. Transverse DIFs in image log. Reproduced from Nelson et al. (2005).

wells are not along the wellbore axis, and are not contained by the perpendicular plane, making the relationship more complicated. Muhajir et al. (2018) analyzed the hole-shape data from caliper logs using the inversion technique to detect the borehole breakouts and DIF. They deduced the *in-situ* stress orientations. Integrated stress analysis inversion was carried out on the data of the DIFs and breakouts were obtained by analyzing borehole images. Caliper log data and borehole image analysis were applied to five wells at the Sukowati field (east Java).

In a deviated borehole DIFs are present as *en-echelon* pairs of fractures at an angle to the borehole wall. As they propagate away from the well, they bend and tend to become perpendicular to S_H. The absence of DIFs in a borehole makes it possible to constrain the upper bounds on the S_H magnitude (Zoback et al., 2003). This was also confirmed by the photoelasticity experiments where photoelasticity lab tests were carried out by simulating the initiation and propagation of DIFs in glass cubes containing borehole at different angles (Jia et al., 2015). In case of a vertical borehole, axial DIFs were formed, and in the 45° plunging borehole, *en-echelon* fractures were observed. This experiment concurred that when one of the principal stress axes is parallel with the borehole, tensile DIFs develop, else *en-echelon* tensile fractures appear.

Okabe et al. (1998) demonstrated the possibility of estimating the stress regime for a drill core related to an inclined borehole using an inversion technique, by taking the sets of the circumferential positions of DIF along the borehole surface and the inclination of small fractures of the DIF. The problem was conducted using synthethic data and was validated by real data taken from a borehole at the Japan Main Island.

Borehole micro-resistivity imagery has been used to study DIFs in horizontal wellbores (Miller et al., 2011). The zones that have lower fracture initiation pressures show more numerous DIFs. There are two types of DIFs that form within a horizontal borehole: transverse and longitudinal, which originate at the top and bottom of the borehole. These are generated in extensional regimes where the overburden stress magnitude exceeds the magnitude of S_H. The longitudinal fractures parallel the length of the wellbore, whereas the transverse DIF parallels the maximum horizontal stress direction, at a high inclination to the borehole length. In country rocks devoid of DIF, a high stress environment and high stress anisotropy are expected (Miller et al., 2011).

5. DIF in image logs (e.g. Fig. 13)

DIFs in drill cores exhibit certain characters as revealed in image logs that give an idea about their origin, orientation, size, spacing, and distribution. DIFs can be identified in image logs as sharply defined narrow features sub-parallel to the borehole axis in a vertical well (Miller et al., 2011). DIFs are poor reflectors of acoustic energy, so they appear as narrow bands of low reflectivity (Asquith and Krygowski, 2004).

Borehole imaging tools are based on contrasts in physical properties of the rock. Resistivity imaging tools utilize the contrast in resistivity between the DIFs and the intact core (Ekstrom et al., 1987, Fig. 14). Since the DIFs get infiltrated by drilling mud, they appear as narrow pairs of conductive features in the resistivity logs separated by 180° and run sub-parallel to the borehole axis in vertical wells. Ma et al. (1993) mapped the acoustic impedance boreholes using an ultrasonic transducer pulse-echo response tool that used 250 kHz to 1.3 MHz frequency, and gives a Borehole Televiewer (BHTV) image with the 360° periphery of the borehole. This enabled excellent mapping and characterization of DIFs. Fig. 15 presents an example of DIFs as deciphered in an acoustic image.

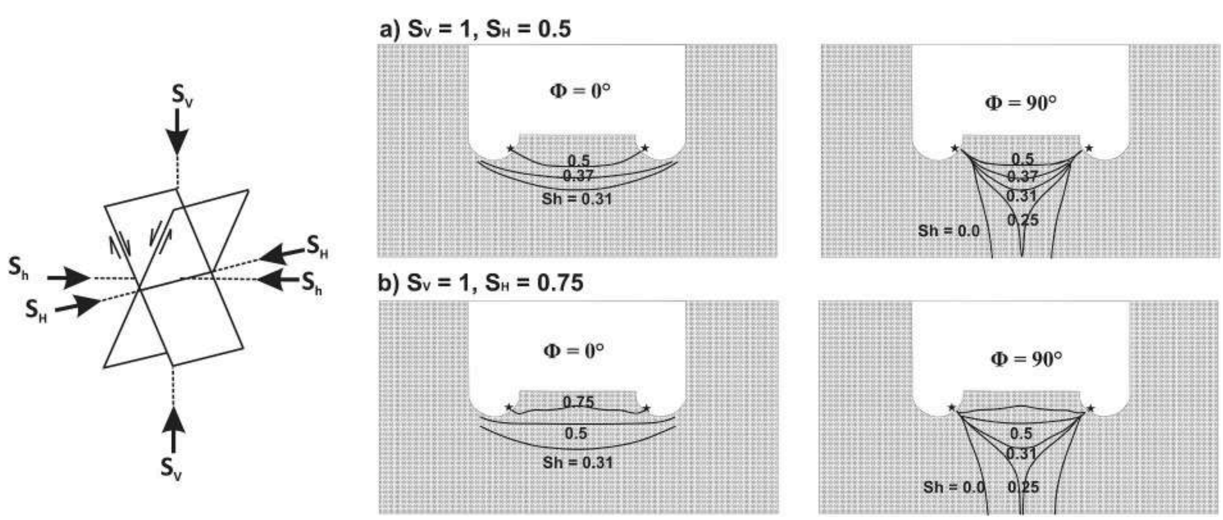

Fig. 9. Predicted trajectories of fractures in the normal fault stress regime. Reproduced from (Li and Schmitt, 1998). Φ = 0° → the cross section is parallel to S_H. Φ = 90 ° → the cross section is perpendicular to S_H. S_H = Maximum horizontal compressive stress. S_h = Minimum horizontal compressive stress. Cross-section: planes passing through the wellbore axis. S_v = Overburden stress. The values of the stresses are normalized and S_v is taken as 1, **(a)** S_v = 1, S_H = 0.5, **(b)** S_v = 1, S_H = 0.75.

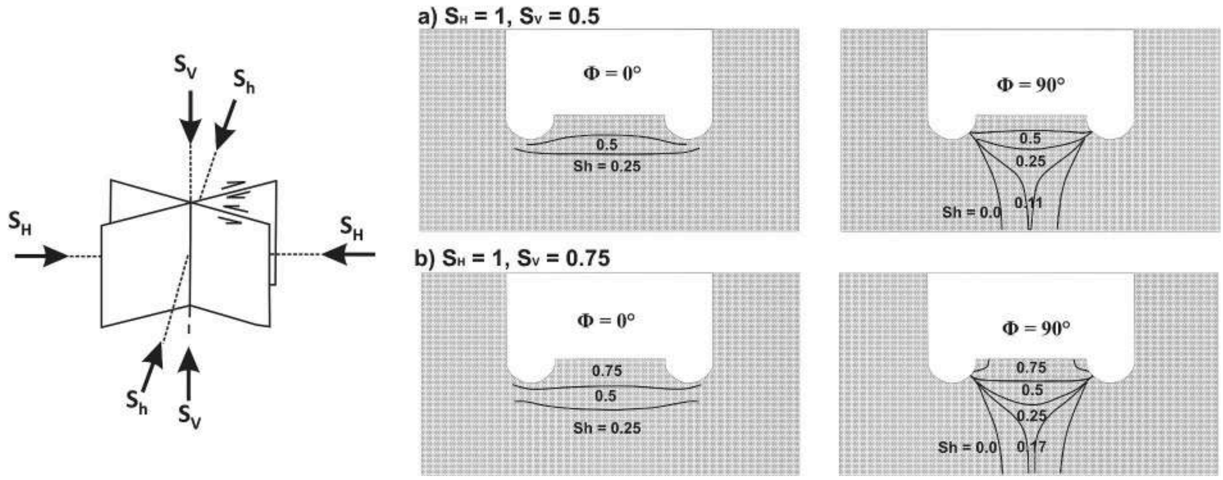

Fig. 10. Predicted trajectories of fractures in the strike-slip fault stress regime. Reproduced from (Li and Schmitt, 1998). Φ = 0° → the cross section is parallel to S_H. Φ = 90 ° → the cross section is perpendicular to S_H. S_H = Maximum horizontal compressive stress. S_h = Minimum horizontal compressive stress. S_v = Overburden stress. The value of the stresses are normalized and S_H is taken as 1, **(a)** $S_H = 1$, $S_V = 0.5$, **(b)** $S_H = 1$, $S_V = 0.75$.

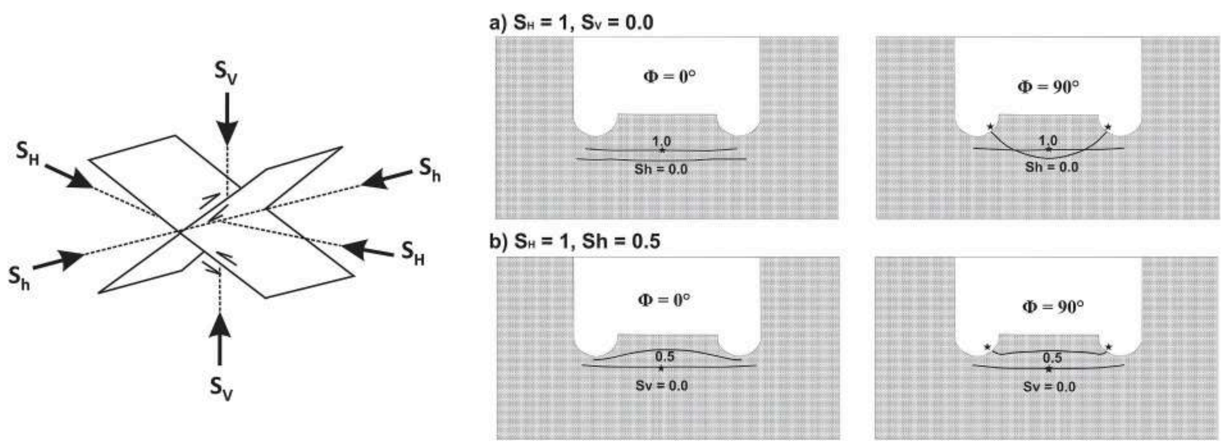

Fig. 11. Predicted trajectories of fractures in the thrust fault stress regime. Reproduced from Li and Schmitt (1998). Φ = 0° → the cross-section is parallel to S_H. Φ = 90° → the cross section is perpendicular to S_H. S_H = Maximum horizontal compressive stress S_h = Minimum horizontal compressive stress. S_v = Overburden stress. The values of the stresses are normalized and S_H is taken as 1, (a) $S_H = 1$, $S_v = 0.0$ (b) (a) $S_H = 1$, $S_h = 0.5$.

Besides the resistivity and acoustic imaging tools, DIFs appear on a number of optical imaging tools, as fine fractures separated by 180°. In bulk density images, DIFs are seen as narrow low-density features subparallel to the borehole axis. In photoelectric absorption factor (Pe), DIFs are imaged as high Pe fracture zones (Tingay et al., 2008, 2016).

Guha et al. (2006) integrated a number of logging while drilling (LWD) logs, LWD propagation resistivity, wireline array induction (HDIL), multi-component induction (3DEX) and cross-dipole acoustic measurements (XMAC Elite) to analyze the fracture intensity, length and orientation in an overbalanced vertical well from offshore India. The presence of DIFs is marked by the large difference between LWD resistivity and array induction resistivity data, separation of the shallow and deep array induction resistivity curves and different responses of multi-component measurements (3DEX). A combination of the multi-sensor sonic and induction log gives better results in characterizing the DIF and reduces the uncertainties. The length of the DIFs are obtained from a High Definition Induction Log (HDIL).

6. Distinguishing natural fractures from DIF

Proper identification of DIFs and their influences on logging not only enhances the geologic and petrophysical understanding, but also enables more efficient drilling. The knowledge of the presence or absence of DIFs allows the use of preventive measures to counter lost circulation, thus enabling more efficient and cost-effective drilling. The petrophysical and geologic interpretations can be improved by distinguishing natural fractures from the induced ones (Plumb et al., 1999). This can be done by geomechanical modeling of failure modes, real time logging while drilling data, annular pressure measurements and resistivity at the bit images (Rezmer-Cooper et al., 2000). Bratton et al. (2001) improved this technique by using real-time resistivity and annular pressure measurements for wells using oil-based muds.

The increase in the density of the DIFs renders interpretation of tectonic/natural fractures difficult. Kulander et al. (1990) and Keren and Kirkpatrick (2016) described ten styles or geometric variations of induced deformation documented in drill cores from the Japan trench (Fig. 16). They used high-resolution imagery of the cores, done using a multi-sensor core logger (MSCL)-I digital imaging system with GEOSCAN IV (Geotek, Ltd.) that involves a linear scanline method to scan the structures. The deformation manifestations are as described below.

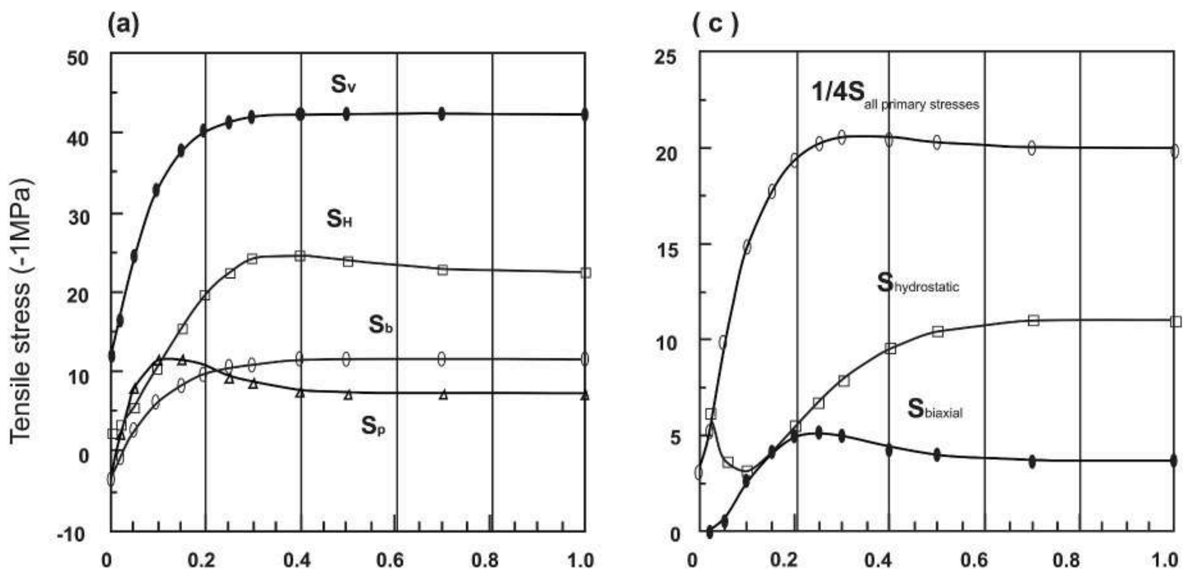

Fig. 12. Relationship between greatest tensile stress and normalized core stub length. Reproduced from Li and Schmitt (1998).

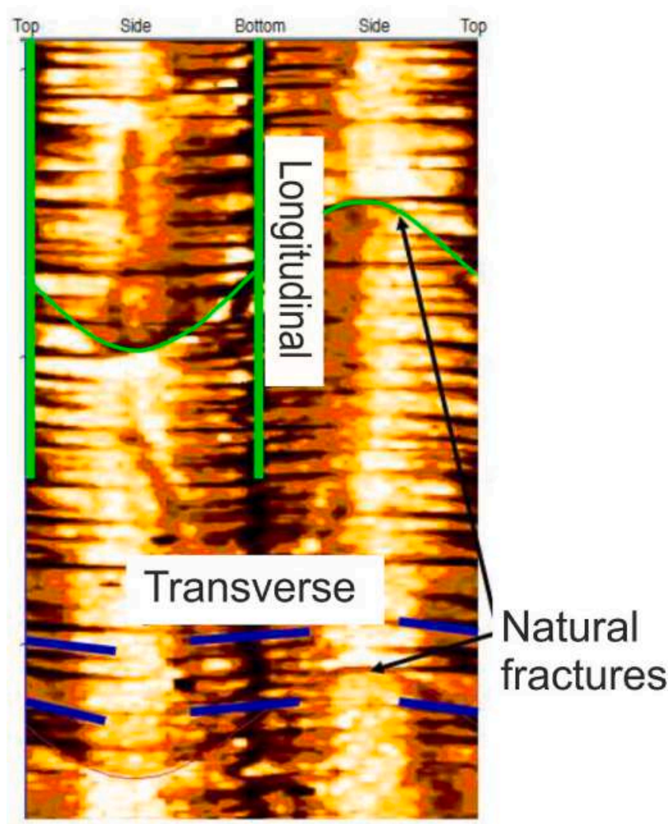

Fig. 13. Natural fracture and longitudinal and transverse DIFs in image log. Reproduced from Miller et al. (2011).

- Drilling biscuits/discs: These are separate blocks formed due to coring, with concave bottoms and/or convex tops, and are usually separated by drilling mud or rock fragments. Inclinations of the edges of the discs are usually horizontal in the vertical borehole, but the orientation can be influenced by the presence of inclined beds (Kulander et al., 1990). Fully developed horizontal biscuits cut across the core or abut against the other fractures. The discs form due to the action of vertical tensile stress due to the removal of overburden (also see Kidd, 1978; Kulander et al., 1990).
- Induced brecciation: Cores containing only broken angular clasts. Such breccias do not posses striations/slickenlines/slickenslides, which distinguish them from several natural clasts.
- Triangular fracture sets: These have orientations parallel to the edge of the biscuits and other induced structures. These fractures form at the split face of the core, at the edge of the core barrel.
- Near right-angle fractures: Continuous fractures showing a high-angle bend (~90°) are observed near the outer edge of the cores, along the biscuit corners. These form as a result of the continuous rotation and flexure of the core.
- Radiating fractures: Fractures that originate from a common point and can display a radial symmetry (Arthur et al., 1980; Dengo, 1982). Similar down-core diverging cured fractures generated at the outside of the core have also been reported (Kulander et al., 1990).
- Core axis parallel fractures: Petal and Petal-centerline fractures parallel the greatest horizontal stress (S_H) (Li and Schmitt, 1998). They are usually seen as down-core dipping fractures in the drill cores. These are used to evaluate the direction and magnitude of the S_H (Fig. 1).
- Fractures crosscutting drilling mud: Such fractures are always drilling-induced, as evident from the relative time relation, i.e., the fracture formed after the drilling injection.

Williams et al. (2016) studied the damage zone of the Alpine fault New Zealand from the X ray computed tomography studies of the drill cores. In order to accurately characterize the damage zone, distinction between the natural and induced fractures in the cores was of utmost importance. Disc fractures, brecciation due to drilling and triangular fracture sets were identified.

7. Applications

7.1. Determination of in-situ stress magnitudes and direction (Fig. 17)

The process of drilling a well results in a concentration of the far-field tectonic stresses closer to the wellbore. Drilling-induced failure occurs when it crosses the rock strength. Using the techniques of logging and wellbore imaging, these failures can be detected and used for the estimation of unknown stress magnitudes. For vertical boreholes, the *in-situ* stress regimes can be constrained if the downhole mud pressure, tensile

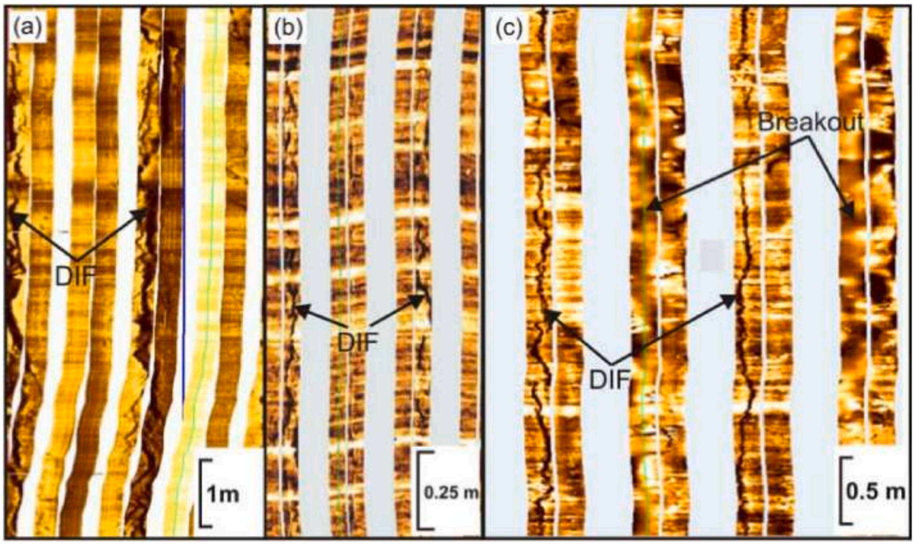

Fig. 14. DIFs deciphered in the Formation Micro Imager (FMI). Reproduced from Ekstrom et al. (1987).

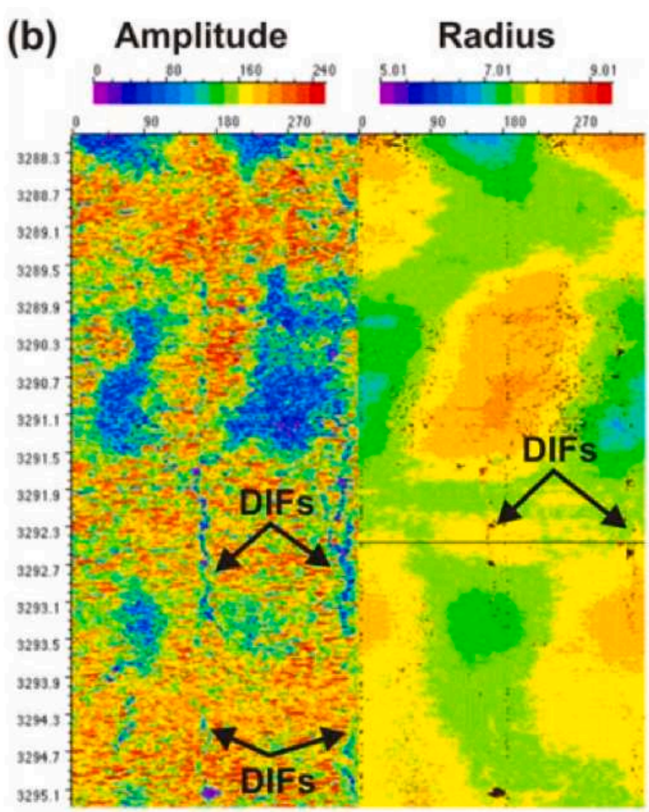

Fig. 15. DIFs in acoustic image. Reproduced from Ekstrom et al. (1987).

strength of the rock to the horizontal tensile stress, and the pore pressure are known. For an inclined borehole, *en-echelon* fractures are drilling-induced on which inversion methods can be applied to constrain the *in-situ* stresses. (Bosworth et al., 2012; Saoudi et al. 2012; Zhang, 2019) (Appendix).

Table 1 Initiation of DIFs have been used to estimate the stress magnitude for rocks with low permeability with negligible pore diffusion. The magnitude of S_H can be derived by studying the timing of the initiation of the fractures. In such a model (Brudy and Kjerholt 1999), two extreme scenarios are considered: when the fracture initiates right after drilling, the magnitude of the S_H is the maximum, and it decreases as the time gap between the drilling and initiation of fracture decreases. It reaches a minimum value when the fracture is considered to be initiated shortly before logging. This model, when applied to determine the state of stress in the northern North Sea region, provided results that were in accordance with previous elastic analysis. However, this model does not explain the effect of the plastic material behavior and the effects caused due to the interaction of drilling mud and shale.

Brudy (1998) provided high quality stress orientation data of the northern North Sea by analyzing DIFs from image logs of 16 wells in the area. Inclined DIF in a vertical borehole indicated that the orientation of the principal stress axis was not vertical. It was also observed that the probability of the occurrence of DIFs increases with the hole depth. This correlates with the increase in stress differences with depth. From the study of the image logs, it was concluded that the area is presently under a strike-slip regime.

Data from offset wells in the Kolosh Formation (northern Iraq) was analyzed in the diagnosing of drilling hazards and predict the possibility of fracturing (Fig. 18). Vertical DIFs were used to determine the S_H orientation (Abalioglu et al., 2011).

A similar application of DIF data was carried out in constructing a 3D geomechanical model for the optimization of drilling in the Llanos Orientales Basin, Colombia. (Araujo et al., 2010). The formation of DIFs near a vertical wall, drilled with mud weight lower than the fracture gradient, indicated the presence of a significant horizontal stress anisotropy and with $S_H > S_V$.

Mazumder et al. (2010) determined the orientations of S_H and S_h in the Baturaja Formation of South Sumatra Basin (Indonesia) using the dominant orientations of breakouts and DIFs determined from FMI images combined with caliper logs.

In the global review of stress regimes in hydrocarbon fields by Zoback et al. (2003), DIFs constrained the lower bound of the S_H magnitude. DIFs form when the following two conditions are met: *(i)* $S_H \gg S_h$, and *(ii)* wellbore pressure exceeds the mud pressure. The mud-induced cooling also affects the genesis of DIFs. For example, cooling of the wellbore originates *en echelon* sets of DIF. However, the influence of the increase in mud weight is more than that of the increase in cooling for the DIFs. Thus, the observation of DIFs can provide a lower bound for the S_H if S_v, S_h and the pore pressure are known (Zoback, 2007).

Allan et al. (2019) modeled the fracture plane in order to plan a sidetrack trajectory of drilling that bypasses the DIFs. This was done by determining and validating the S_H orientation and detection of the

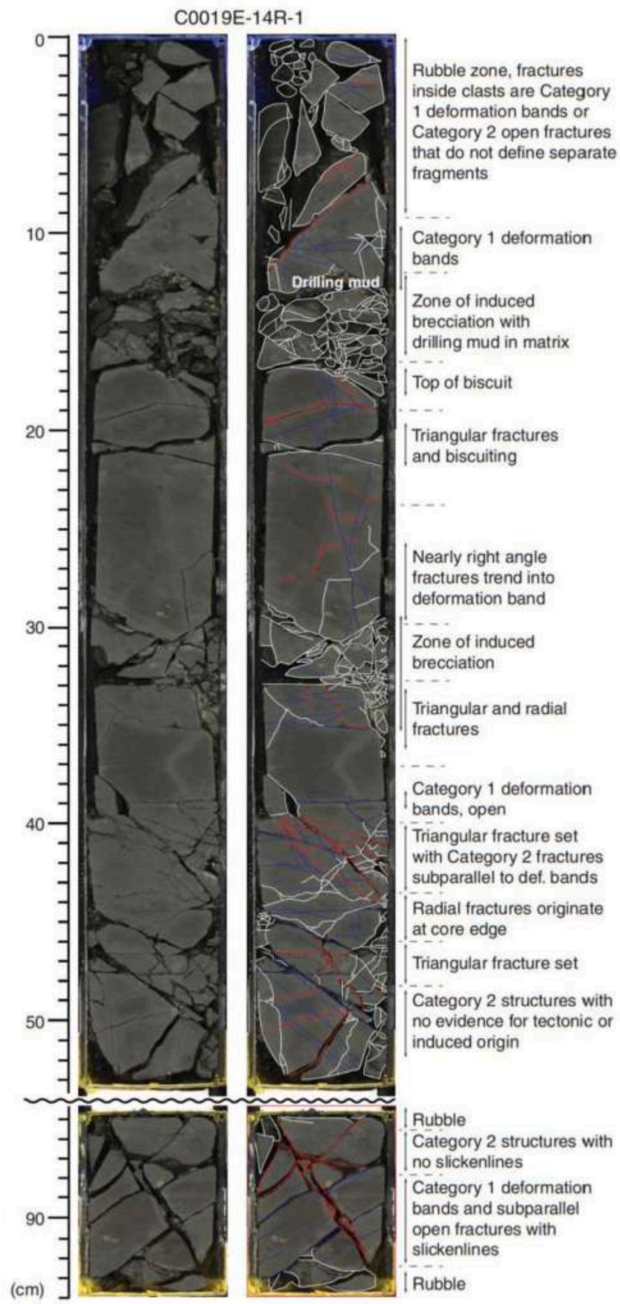

Fig. 16. Core section from Japan trench digitized to show the different fractures and deformation. Reproduced from Keren and Kirkpatrick (2016).

fracture. A sidetrack trajectory was calculated to minimize the chances of encountering the fractured zone. The model was applied to the borehole at the Shah Deniz field (South Caspian Sea) by considering the stress regime and the pore pressure.

Higgins et al. (2006) presented a 1D geomechanical model of the stress regime to optimize the production at Rulison field (USA). From the image log data, S_H was considered to parallel the DIFs. This was achieved by forward modeling the DIFs and the far field stresses were converted to the near wellbore stresses to estimate the failure.

Wilson et al. (2007) documented the natural and induced fractures from the cores of the McMurdo Ice shelf (Antarctica). The documentation was done by scanning the whole core/intact segments. DIFs include steeply dipping, petal, petal-centerline, core-edge induced fractures and sub-horizontal induced extension fractures. The density of petal centerline fractures decrease towards the bottom of the core. A number of sub-horizontal fractures are encountered with circular grooves along which the cores have rotated.

Wiprut et al. (1997) employed the interactive software system of *Stress and Failure of Inclined Boreholes* (SFIB, Peska and Zoback, 1996), to study the compressive and tensile DIFs in a wellbore at the Visund oil field (Norway) to constrain the *in situ* stress regime. They also reviewed conditions for wellbore instability and sand production. It was observed using FMI that the orientations of the DIFs match with observations made using other methods. The data from compressive and tensile DIFs have been used to present a complete stress tensor model. Next, an estimation of the rock strength and optimal wellbore trajectories was also proposed.

Bankwitz and &Bankwitz (1997) studied the drilling-induced

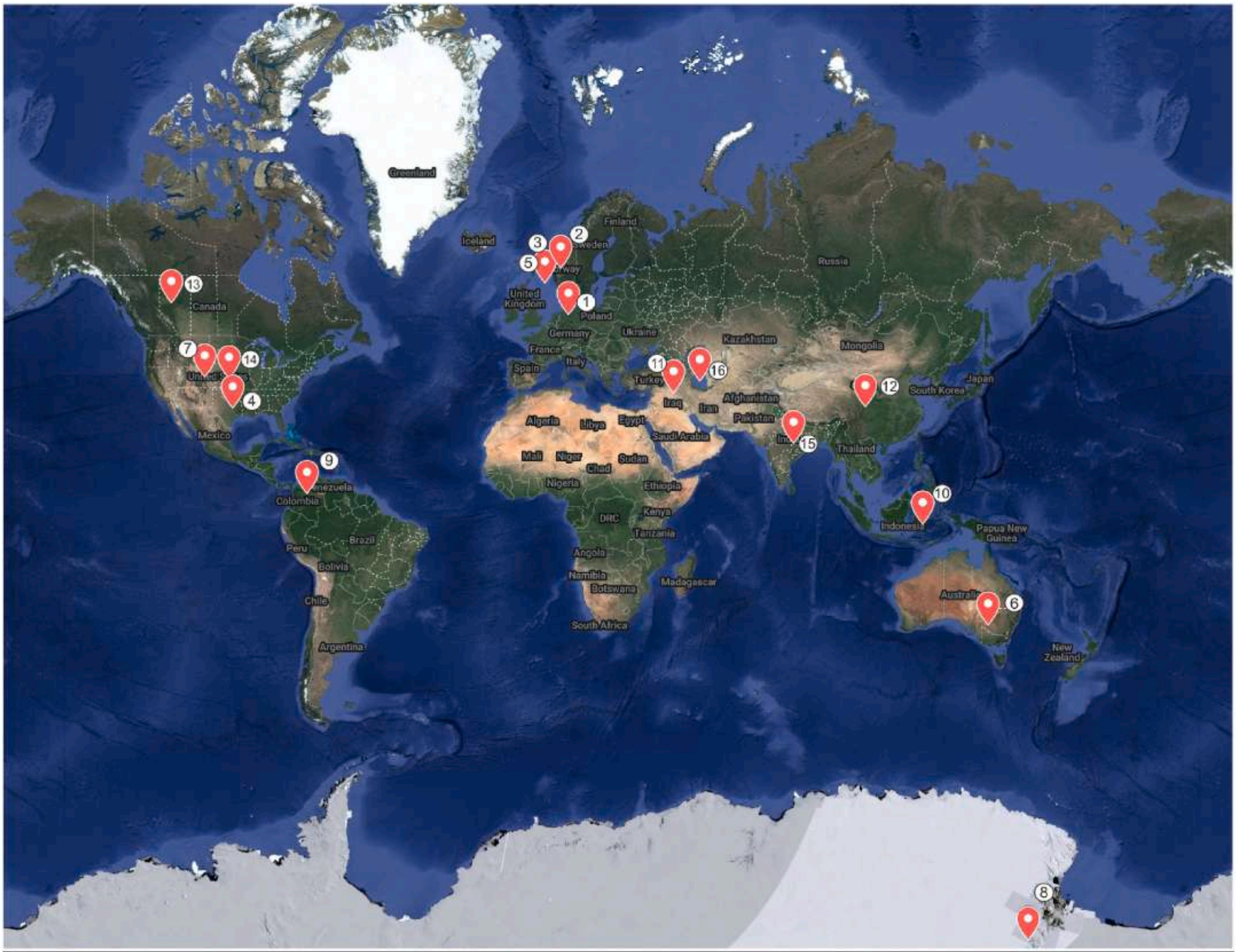

Fig. 17. World map showing the regions where DIFs have been used to determine the stress regime. Numbers refer to Table 1.

features in the German Continental Deep Drilling Project (KTB) related drill cores to determining the present-day stress field in the Bohemian massif (Germany). Formation MicroImager and FMS/Formation Micro Scanner log data were used to study the 3D shape and symmetry of the fractographic features in the borehole. The strike of the bifurcating centerline fractures were used to determine the orientation of the maximum horizontal stress up to 7800 m depth. The high density of disk fractures was presumably a result of the superposition of additional tectonic stress.

Nie et al. (2013) analyzed fractures in the borehole wall using resistivity and acoustic image logs to determine the *in situ* stress from the DIFs in the Wenchuan Earthquake fault zone (China). This was done to investigate the distribution of the fault zones and study the earthquake mechanism. Core samples and image log data were obtained from four boreholes drilled in the maximum displacement region by the Wenchuan Earthquake Fault Scientific Drilling Project (WFSD).

Titheridge (2014) proposed a technique to determine the angle between face cleat and the principal horizontal stresses (S_H, S_h) using the DIFs (petal, core edge, disc and saddle fractures) present in the coal core. This further enabled to interpret the orientation of the face cleat, which was important to know for the CO_2 sequestration and planning the direction of hydro-fractures low-permeability areas. This method applies to coal beds and coal mines.

Chatterjee and Singha (2018) identified DIFs from borehole image logs in the Krishna-Godavari basin to find the orientation of S_H, and further studied the rock mechanical properties. Laubach et al. (1988) determined the orientation of the petal-centerline fractures and used it to interpret the present-day stress regime in East Texas (USA). S_H and S_h directions were further used to deduce the trajectory of the induced hydraulic fracturing done in that area. The agreement between the DIFs and the natural fractures indicated that paleo and present stress regimes resemble each other.

Schwab et al. (2017) studied the well log images of the DIFs to determine the present day S_H and S_h in the Wellington and Anson Bates field (USA). The study was carried out to determine the potential of earthquakes caused due to the injection of CO_2 in reservoir for storage and enhanced oil recovery. The DIFs indicated that the maximum horizontal stress direction was along E-W direction. It was concluded that high rates of CO_2 injection could potentially reach the threshold pressure of failure in the region.

Patlan et al. (2008) studied the DIFs from the cores and acoustic image logs and borehole televiewer images of borehole from the Victoria Land rift basin (Antarctica) to determine the present day stress fields. The software CoreBAse was used to stitch the core section logs into a cumulative image of the whole core. WellCAD software was used to determine the orientation of the DIFs, which then provided the direction of maximum horizontal stress in this area.

Table 1
List of works that have used DIFs to determine the stress regimes in the region.

Sl. No.	Author	Work	Region	Methods
1	Bankwitz & Bankwitz (1996)	Present day stress orientations	Bohemian massif (Germany)	FMI Microscanner
2	Wiprut et al. (1997)	Stress tensor modelling	Visund field, Norway	SFIB software
3	Brudy (1998)		Northern North Sea	Image logs
4	Zhang (2019)	Study of induced hydraulic fracturing	East Texas (USA)	Image logs
5	Brody and Kjorholt (1999)	Modelling the origin of DIFs	Northern North Sea	Well logs
6	Nelson et al. (2005)	Interpreting DIFs from image logs	Gippsland Basin, Australia	Formation Microimager
7	Higgins et al. (2006)	Production optimisation	Rulison field (USA).	Image and dipole sonic logs
8	Patlan et al. (2008)	Present day stress fields	Victoria Land Basin, Antarctica	CoreBASE, WELLCAD
9	Araujo et al. (2010)	3D model for drilling optimisation	Llanos Orientales Basin, Colombia	Density and Sonic logs
10	Mazumder et al. (2010)	DIF in coal beds	South Sumatra Basin, Indonesia	FMI, caliper logs
11	Abalioglu et al. (2011)	Diagnosing drilling hazards	Northern Iraq	
12	Nie et al. (2013)	Investigation of fault zones	Wenchuan, China	Acoustic image logs
13	Titheridge (2014)	Orientations of cleats in coal core, implications in CO_2 sequestration	Alberta, Canada	Acoustic and resistivity logs
14	Schwab et al. (2017)	Potential for injection-induced earthquakes	Wellington field, USA	Well image logs
15	Chatterjee & Singha (2018)	Study of rock mechanical properties	Krishna-Godavari Basin, India	Well image logs
16	Allan et al. (2019)	Drilling optimization	South Caspian Sea	Caliper logs, Image logs, LWD image logs, X-dipole sonic logs
17	Radwan et al. (2021)	Developing Pore Pressure Fracture Gradient Model	Southern Gulf of Suez, Egypt	FMI logs, DIFs and borehole breakouts
18	Banerjee & Chatterjee, (2022)	Pore Pressure and stress analysis	Raniganj Basin, India	Resistivity logs, Seismic data, sonic logs

7.2. Analysis and prevention of lost circulation

The development of preventive measures, viz., enhanced hydraulics and geomechanical models, new field techniques and new lost circulation materials have been the strategies for addressing DIFs. DIFs can form in a low-pressure reservoir caused by pressure depletion or pore pressure regression. It also induces a lower fracture gradient. To prevent the formation of DIFs, these risky zones are identified and low mud weight is maintained. Since the stress configuration around the inclined boreholes differs spatially, fracture widths vary with the direction of drilling (Feng and Gray, 2018).

Feng and Gray (2018) modeled the fluid loss caused by DIFs in a dynamic circulation pressure environment using the finite-element method. The simulation takes care of dynamic mud circulation in the wellbore and gives an estimate of time-dependent wellbore pressure, fluid-loss rate, fracture profile during drilling and the boundary conditions of the bottomhole pressure. The mud viscosity has a greater impact on the fracture width whereas the pump rate affects the length more.

Lost circulation has been used in the detection of fractures as well. Wutherich et al. (2020) presented a method of detecting DIFs by analyzing the amount of energy spent during the drilling of a well. The depletion around a fractured zone increases the differential pressure between the wellbore and the formation. This increases the energy required to drill the region, which gives the location of the fracture. This method has been applied and validated by using field data from over seventy wells.

Drilling of a well requires the selection of mud with a suitable density that balances the pressure from the formation fluids but does not exceed the pressure that initiates fractures. For a very high-density mud, the minimum hoop stress exceeds the tensile strength and DIFs form, whereas if the mud density is too less, the maximum hoop stress exceeds the compressional strength and results in the formation of borehole breakouts (Gu et al. 2017). After DIFs form, the fractures zones cause loss of a large amount of circulating fluids. To prevent this loss due to DIFs, several avenues have been postulated-refining of hydraulic and geo-mechanical models, new field techniques and new lost circulation materials such as cross-linked polymer pills, gunk squeezes and cement squeezes, water and synthetic based muds (Brege et al., 2010).

Wang et al. (2019) performed a 3D finite element analysis using COMSOL to study the applicability of non-isothermal wellbore strengthening to increase the effectiveness combating lost circulation in boreholes with DIFs.

8. Discussions

A combination of resistivity, acoustic, optical image logs and Logging while drilling data can efficiently characterize the DIFs. Relying solely on the retrieved core fragments to decipher DIF render considerable doubt as the retrieval process might result in loss of fragments and corresponding information. Removal of noise in the image log data, and increase in the resolution of the data would make the identification of DIF easier. Better scanning devices, more efficient core retrieving methods and more accurate characterization of the pressure and resistivity measurements inside the boreholes would lead to identification of DIFs more accurately.

The damage caused by the DIFs tends to increase as the borehole increases in size, and the weaker rocks are more damaged than the stronger rocks. Stronger rocks drilled with small bits show the evidence of less damage than the weaker rocks drilled with large bits (Feng and Gray, 2018). Borehole breakouts and DIFs have been used to determine ~19% of the stress orientations in the World Stress Map (WSM) database (Heidback et al. 2016). Additionally, the majority of stress orientation indicators in petroleum and geothermal systems are usually provided by borehole breakouts and DIFs (Tingay et al., 2008). Repository presents factors affecting genesis of DIFs in country rocks.

9. Future works

Although significant work has been done on DIFs and their characteristics, a number of research questions need to be addressed. These are: *(i)* 3D visualization of DIFs in cores. *(ii)* A detail understanding of DIFs developed in inclined and horizontal drill cores and boreholes in terms of forward modeling. Inclined boreholes have a more complicated relation between the principal stresses and the wellbore axes. Visualization and modeling of DIFs in cores from horizontal boreholes is required because it would lead to a better understanding of the hydraulic fracturing mechanism and find application in several oil and gas fields. *(iii)* Accurate analytical models explaining the growth and propagation of the DIFs in the core. *(iv)* More accurate detection of DIFs in image logs. This will lead to better prevention strategies and treatment plans for dealing with lost circulation in fractured reservoirs.

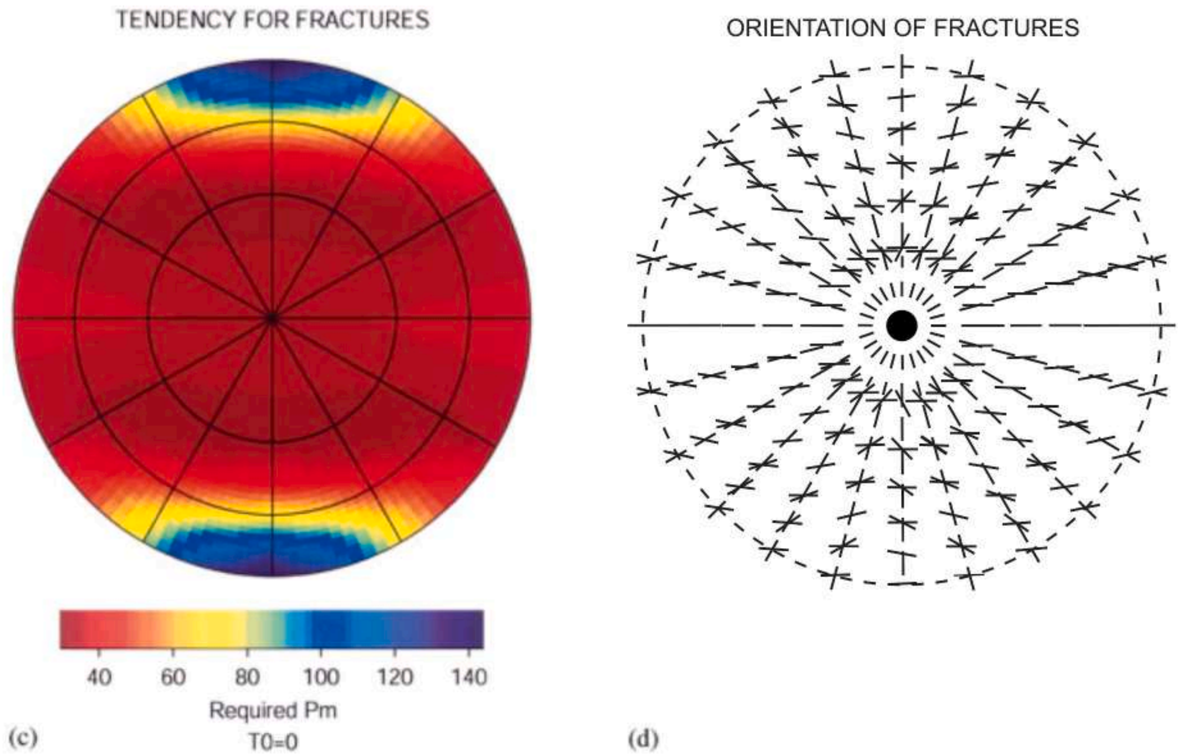

Fig. 18. Tendency of DIF initiation in terms of excess mud weight needed, and orientation of DIF in plan view. Colors indicate the required excess mud weight. Reproduced from Zoback et al. (2003). (For interpretation of the references to colour in this figure legend, the reader is referred to the Web version of this article.)

10. Conclusions

DIFs develop parallel to the direction of S_H and perpendicular to S_h. Based on this, the principal stress directions can be worked out from the DIFs. Tensile fractures occur when the stress exceeds the tensile strength of the rock. Thus, the study of DIFs can give an idea about the magnitude of the stresses as well.

The factors affecting the formation of DIFs are the rock anisotropy, mud density, stress anisotropy, grain size and orientation of the rock, interaction between the grains, breakage mechanism and mechanical properties of the formation, drill type, bit size and the energy transferred to the borehole while drilling.

Distinguishing natural fractures from DIFs is important to decipher the principal stresses, modeling lost circulation or characterizing the damage zone of faults. The anisotropy in the principal horizontal stresses (S_H –S_h) can be quantified from the type of DIF present in the core. Greater the depth more close-spaced are the DIFs. Modeling of the lost circulation of drilling mud using models is one of the industrial applications of DIFs. Artificial neural models are in use to predict the amount of lost circulation before the drilling process begins by incorporating the data of DIFs.

Further studies on DIFs are needed regarding *(a)* horizontal and inclined drill cores, *(b)* growth of such fractures and *(c)* improved recognition of such fractures from (image) logs.

Declaration of competing interest

The authors declare that they have no known competing financial interests or personal relationships that could have appeared to influence the work reported in this paper.

Data availability

It is a review article. No original data presented.

Acknowledgements

CPDA grant (IIT Bombay) supported SM. SC worked as a self-funded summer intern with SM in 2021 in online mode. Dr. Mohit Kumar Puniya (Survey of India, Dehradun) kindly drafted several figures. We thank Subhobroto Mazumder (Oil and Natural Gas Corporation) and Lucie Novakova (Institute of Rock Structure and Mechanics of the CAS) for reviewing the article. Tiago Alves (Cardiff University) handled this article.

Appendix A. Supplementary data

Supplementary data to this article can be found online at https://doi.org/10.1016/j.marpetgeo.2022.106089.

Appendix

How to constrain *in-situ* stress (Zhang, 2019):

For vertical boreholes, the *in-situ* stress conditions can be constrained if the downhole mud pressure (P_m), tensile strength of the rock to the horizontal tensile stress (T_0), and the pore pressure (P_p) are known. When the DIFs initiate, it can be assumed that the downhole mud pressure is equal to the formation initiation pressure. This is used to calculate the maximum horizontal stress direction in a vertical well under normal and strike-slip regimes. When the rock starts to fail,

$$S_H > 3^*S_h - P_m - P_p + T_0 \quad (1)$$

This inequation is plotted on the stress polygon diagram and when combined with other methods like borehole breakouts, the stress conditions can be constrained.

References

Aadnoy, B.S., Bell, J.S., 1998. Classification of DIFs and their relationship to in-situ stress directions. Log. Anal. 39, 27–42.

Abalioglu, I., Legarre, H., Garland, C., Sallier, B., Gao, J., van Galen, M., Chou, Q., Neil, B., Soroush, H., Qutob, H., Mahli, Z., 2011. The role of geomechanics in diagnosing drilling hazards and providing solutions to the northern Iraq fields. SPE Middle East Oil and Gas Show and Conference 142022, 1–11.

Allan, F., Shepherd, D., Abbasov, A., Villinski, J., Majidi, R., Bagir, I., 2019. Modelling of Fracture Geometry to Reduce the Risk of Intercepting Drilling Induced Fractures when Designing Sidetrack Trajectories. SPE Annual Caspian Technical Conference. OnePetro. SPE-198384-MS.

Araujo, E., Alcalde, R., Mateus, D., Fernandez-Ibañez, F., Sheridan, J., Ward, C., Brudy, M., Alvarellos, J., Ordonez, L.Y., Cardona, F., 2010. Drilling optimization using 3D geomechanical modeling in the Llanos Orientales basin, Colombia. In: SPE Latin American and Caribbean Petroleum Engineering Conference. https://doi.org/10.2118/0911-0086-JPT. OnePetro.

Arthur, M.A., Carson, B., von Huene, R., 1980. Initial tectonic deformation of hemipelagic sediment at the leading edge of the Japan convergent margin. In: Langseth, M., Okada, H., et al. (Eds.), Initial Reports of the Deep Sea Drilling Project, vol. 56. U.S. Government Printing Office), Washington, DC, p. 57, 569–613.

Asquith, G., Krygowski, D., 2004. Basic well log analysis. In: AAPG Methods in Exploration, vol. 16. AAPG, Tulsa, Oklahoma, p. 244.

Banerjee, A., Chatterjee, R., 2022. Pore pressure modeling and in situ stress determination in Raniganj basin, India. Bull. Eng. Geol. Environ. 81 (1), 1–18.

Bankwitz, P., Bankwitz, E., 1997. Fractographic features on joints in KTB drill cores as indicators of the contemporary stress orientation. Geol. Rundsch. 86, S34–S44.

Bosworth, W., Khalil, S., Clare, A., Comisky, J., Abdelal, H., , Reed, T, Kokkoros, G., 2012. Integration of outcrop and subsurface data during the development of a naturally fractured Eocene carbonate reservoir at the East RasBudran concession, Gulf of Suez, Egypt. In: Spence, G.H., Redfern, J., Aguilera, R., Bevan, T.G., Cosgrove, J.W., Couples, G.D., Daniel, J.-M. (Eds.), Advances in the Study of Fractured Reservoirs, vol. 374. Geological Society, London, Special Publications, pp. 333–359.

Bratton, T.R., Rezmer-Cooper, I.M., Desroches, J., Gille, Y.E., Li, Q., McFayden, M., 2001. How to diagnose drilling induced fractures in wells drilled with oil-based muds with real-time resistivity and pressure measurements. In: SPE/IADC Drilling Conference. https://doi.org/10.2118/67742-MS. OnePetro.

Brege, J.J., Christian, C., Quintero, L., Clark, D., 2010. Improving Wellbore Strengthening Techniques by Altering the Wettability of Non-aqueous Fluids Lost to Drilling Induced Fractures. AADE Fluids Conference and Exhibition, Houston, Texas, pp. 6–7.

Brudy, M., 1998. Determination of the state of stress by analysis of DIFs-results from the northern North Sea. In: SPE/ISRM Rock Mechanics in Petroleum Engineering. OnePetro. SPE-47236-MS.

Brody, M., Kjorholt, H., 2018. The initiation of drilling-induced tensile fractures and their use for the estimation of stress magnitude. In: The 37th US Symposium on Rock Mechanics (USRMS). OnePetro.

Brudy, M., Kjorholt, H., 1999. The initiation of drilling-induced tensile fractures and their use for the estimation of stress magnitude. In: Vail Rocks 1999, the 37th US Symposium on Rock Mechanics (USRMS). OnePetro. ARMA-99-1189.

Chatterjee, R., Singha, D.K., 2018. Stress orientation from image log and estimavtion of shear wave velocity using multiple regression model: a case study from Krishna—godavari basin, India. J Indian Geophys Union 22, 128–137.

Dengo, C., 1982. A structural analysis of cores from the Leg 67 transect across the Middle America Trench—offshore Guatemala. In: Aubuoin, J., von Huene, R., et al. (Eds.), Initial Reports of the Deep Sea Drilling Project, vol. 67. U.S. Government Printing Office), Washington, DC, pp. 651–666.

Ekstrom, M.P., Dahan, C.A., Chen, M.Y., Lloyd, P.M., Rossi, D.J., 1987. Formation imaging with microelectrical scanning arrays. Log. Anal. 28, 294–306.

Feng, Y., Gray, K.E., 2018. Modeling lost circulation through DIFs. SPE J. 23, 205–223.

Gu, M., 2017. Impact of anisotropy induced by shale lamination and natural fractures on drilling, completion, and fracturing design. In: SPE/AAPG/SEG Unconventional Resources Technology Conference (OnePetro).

Guha, R., Tyagi, A.K., Corley, B., Rabinovich, M., Tang, X., 2006. Integrating multi-sensor acoustic and resistivity data for improved formation evaluation in the presence of drilling induced fractures. In: SPWLA 47th Annual Logging Symposium. Society of Petrophysicists and Well-Log Analysts.

Heidback, O., Rajabi, M., Reiter, K., Ziegler, M., WSM Team., 2016. World stress Map database release 2016. GFZ Data Services. https://doi.org/10.5880/WSM.2016.001.

Higgins, S., Davis, T.L., Bratton, T., 2006. Geomechanical modeling as a reservoir characterization tool at Rulison field, piceance basin, Colorado. In: SEG Technical Program Expanded Abstracts. Society of Exploration Geophysicists, pp. 1683–1687.

Jia, Q., Schmitt, D.R., Kofman, R., Chen, X., 2015. Understanding the Mechanical Behavior of Drilling-Induced Tensile Fractures through Photoelasticity Lab Tests Conducted on Glass Cubes. GeoConvention.

Keren, T.T., Kirkpatrick, J.D., 2016. Data report: tectonic and induced structures in the JFAST core. Proc. IODP 343, 343T.

Kidd, R.B., 1978. Core-discing and other drilling effects in DSDP Leg 42A Mediterranean sediment cores. In: Hsu, K., Montadert, L., et al. (Eds.), Initial Reports of the Deep Sea Drilling Project, 42 Part 1. U.S. Government Printing Office), Washington, DC, pp. 1143–1149.

Kostov, N., Gosavi, S.V., Kulkarni, K., Dasari, G., 2016. Fracture Modeling for Optimum Wellbore Integrity Enhancement. Abu Dhabi International Petroleum Exhibition & Conference. OnePetro. SPE-183325-MS.

Kulander, B.R., Dean, S.L., Ward, B.J., 1990. Fractured core analysis: interpretation, logging, and use of natural and induced fractures in core. In: Methods in Exploration Series Number 8. American AFssociation of Petroleum Geologists, Tulsa.

Laubach, S.E., Monson, E.R., 1988. Coring-induced fractures: indicators of hydraulic fracture propagation in a naturally fractured reservoir. In: SPE Annual Technical Conference and Exhibition. OnePetro. SPE18164.

Li, Y., Schmitt, D.R., 1997. Well-bore bottom stress concentration and induced core fractures. AAPG (Am. Assoc. Pet. Geol.) Bull. 81, 1909–1925.

Li, Y., Schmitt, D.R., 1998. Drilling-induced core fractures and *in situ* stress. J. Geophys. Res. 103, 5225–5239.

Lorenz, J.C., Cooper, S.P., 2017. Atlas of Natural and Induced Fractures in Core. John Wiley & Sons, Hoboken, ISBN 978-1-119-16000-7.

Lorenz, J.C., Finley, S.J., 1988. Significance of drilling-and coring-induced fractures in Mesaverde core, northwestern Colorado. No. SAND-88-1623. Sandia National Labs, Albuquerque, NM (USA).

Ma, T.A., Lincecum, V., Reinmiller, R., Mattner, J., 1993. Natural and induced fracture classification using image analysis. In: SPWLA 34th Annual Logging Symposium. OnePetro. SPWLA-1993-J.

Mazumder, S., Sosrowidjojo, I.B., Ficarra, A., 2010. In: The Late Miocene Coalbed Methane System in the South Sumatra Basin of Indonesia. SPE Asia Pacific Oil and Gas Conference and Exhibition. OnePetro. SPE-133488-MS.

Miller, C., Waters, G., Rylander, E., 2011. Evaluation of Production Log Data from Horizontal Wells Drilled in Organic Shales. North American Unconventional Gas Conference and Exhibition. https://doi.org/10.2118/144326-MS. OnePetro.

Morin, R.H., Flamand, R., 1999. Analysis of stress-induced oval fractures in a borehole at Deep Sea Drilling Project Site 504, eastern equatorial Pacific. J. Geophys. Res. Solid Earth 104 (B2), 2767–2775.

Muhajir, Merza Media A, Juandi, D., 2018. A Novel Technique to Correct Horizontal Present Day In-situ Stresses Orientation in Deviated Wells in Sukowati Field, East Java. In: The 2nd SPWLA Asia Pacific Technical Symposium – Indonesia.

Nelson, E.J., Meyer, J.J., Hillis, R.R., Mildren, S.D., 2005. Transverse drilling-induced tensile fractures in the West Tuna area, Gippsland Basin, Australia: implications for the in situ stress regime. Int. J. Rock Mech. Min. Sci. 42 (3), 361–371.

Nie, X., Zou, C., Pan, L., Huang, Z., Liu, D., 2013. Fracture analysis and determination of in-situ stress direction from resistivity and acoustic image logs and core data in the Wenchuan Earthquake Fault Scientific Drilling Borehole-2 (50–1370 m). Tectonophysics 593, 161–171.

Okabe, T., Hayashi, K., Shinohara, N., Takasugi, S., 1998. Inversion of drilling-induced tensile fracture data obtained from a single inclined borehole. Int. J. Rock Mech. Min. Sci. 35, 747–758.

Patlan, E., Wilson, T.J., Millan, C., 2008. Drilling Induced Fracture (DIF) Characterization and Stress Pattern Analysis of the Southern McMurdo Sound (SMS) Core, Victoria Land Basin, Antarctica. AGU Fall Meeting Abstracts, 2008. U13B-0055.

Peska, P., Zoback, M.D., 1996. Stress and Failure of Inclined Boreholes. Stanford University.

Plumb, D., Krabbe, H., Rasmus, J., Li, Q., Bornemann, T., Bratton, T., 1999. Logging-While-Drilling Images for Geomiechanical, Geological and Petrophysical Interpretations. SPWLA 40th Annual Logging Symposium. OnePetro.

Radwan, A.E., Abdelghany, W.K., Elkhawaga, M.A., 2021. Present-day in-situ stresses in Southern Gulf of Suez, Egypt: Insights for stress rotation in an extensional rift basin. J. Struct. Geol. 147, 104334.

Rezmer-Cooper, I., Bratton, T., Krabbe, H., 2000. The use of resistivity-at-the-bit images and annular pressure while drilling in preventing drilling problems. SPE Drill. Complet. 16, 35–42.

Saoudi, A., Moustafa, A.R., et al., 2012. Dualporosity fractured Miocene syn-rift dolomite reservoir in the Issaran Field (Gulf of Suez, Egypt): a case history of the zonal isolation of highly fractured water carrier bed. In: Spence, G.H., Redfern, J., Aguilera, R., Bevan, T.G., Cosgrove, J.W., Couples, G.D., Daniel, J.-M. (Eds.), Advances in the Study of Fractured Reservoirs, vol. 374. Geological Society, London, Special Publications, pp. 379–394.

Schwab, D.R., Bidgoli, T.S., Taylor, M.H., 2017. Characterizing the potential for injection-induced fault reactivation through subsurface structural mapping and stress field analysis, Wellington Field, Sumner County, Kansas. J. Geophys. Res. Solid Earth 122, 10–132.

Tingay, M., Reinecker, J., Müller, B., 2008. Borehole Breakout and Drilling-Induced Fracture Analysis from Image Logs. World Stress Map Project, pp. 1–8.

Tingay, M., Reinecker, J., Müller, B., 2016. 5 Guidelines for Borehole Breakout and Drilling-Induced Fracture Analysis from Image Logs, vol. 33. World Stress Map Project.
Titheridge, D., 2014. Drilling induced fractures in coal core from vertical exploration well: a method to determine cleat azimuth, and the angle between cleat and maximum horizontal stress, and its application. In: Naj, A., Kininmonth, B. (Eds.), Proceedings of the 2014 Coal Operators' Conference, Mining Engineering. University of Wollongong, pp. 1–17.
Wang, Z., Yang, M., Chen, Y., 2019. Numerical modeling and analysis of induced thermal stress for a non-isothermal wellbore strengthening process. J. Petrol. Sci. Eng. 175, 173–183.
Williams, J.N., Toy, V.G., Massiot, C., McNamara, D.D., Wang, T., 2016. Damaged beyond repair? Characterising the damage zone of a fault late in its interseismic cycle, the Alpine Fault, New Zealand. J. Struct. Geol. 90, 76–94.
Wilson, T.J., Paulsen, T., Läufer, A.L., Millan, C., 2007. Fracture Logging of the AND-1B Core, McMurdo Ice Shelf Project, Antarctica, vol. 44. ANDRILL Research & Publications.
Wiprut, D., Zoback, M., Hanssen, T.H., Peska, P., 1997. Constraining the full stress tensor from observations of drilling-induced tensile fractures and leak-off tests: application to borehole stability and sand production on the Norwegian margin. Int. J. Rock Mech. Min. Sci. 34, 365 e1-365.e12.
Wutherich, K., Katon, W., Sinosic, B., Srinivasan, S., 2020. Detecting induced fractures using drilling data to gain insights into unconventional fracture growth. In: SPE/AAPG/SEG Unconventional Resources Technology Conference. https://doi.org/10.15530/urtec-2020-2977. OnePetro.
Zhang, J.J., 2019. Applied Petroleum Geomechanics. Gulf Professional Publishing, 978-0-12-814814-3.
Zoback, M.D., 2007. Reservoir Geomechanics. Cambridge University Press, 9780511586477.
Zoback, M.D., Barton, C.A., Brudy, M., Castillo, D.A., Finkbeiner, T., Grollimund, B.R., Moos, D.B., Peska, P., Ward, C.D., Wiprut, D.J., 2003. Determination of stress orientation and magnitude in deep wells. Int. J. Rock Mech. Min. Sci. 40, 1049–1076.